PHYSICAL REVIEW B VOLUME 8, NUMBER 9 1 NOVEMBER 1973

Magnetic, Transport, and Nuclear-Magnetic-Resonance Properties of $U_{1-x}Pu_xAl_2$ [†]

A. J. Arko, F. Y. Fradin, and M. B. Brodsky
Argonne National Laboratory, Argonne, Illinois 60439

(Received 11 May 1973)

Magnetic-susceptibility, electrical-resistivity, and ^{27}Al Knight-shift and spin-lattice-relaxation results on the pseudobinary cubic Laves phase compounds $U_{1-x}Pu_xAl_2$ are presented. Samples in the annealed and in the self-irradiation-damaged state were studied. The results are consistent with spin fluctuations of the 5*f* electron state associated with the actinide ions. The strength of the coupling between the *s*-wave conduction electrons at the Fermi energy and the 5*f* state is found to increase rapidly with plutonium concentration. In atomically well ordered $PuAl_2$ the coherence of the *s*-*f* hybridization is destroyed by spin-fluctuation scattering above 10 °K. The 5*f* states behave as incoherent virtual bound states centered at the Fermi level in damaged $PuAl_2$ and the Pu-rich alloys. Antiferromagnetic order is found at 6 °K for $U_{0.7}Pu_{0.3}Al_2$.

I. INTRODUCTION

The early members of the 5*f*-electron "actinide" series do not form localized magnetic moments nor order magnetically in the pure metallic state, presumably because the 5*f* electrons overlap to form narrow bands.[1] In some alloys and many intermetallic compounds local moments do exist on the actinide atoms, and long-range magnetic ordering occurs. This is due in part to the larger actinide-actinide distance which reduces the 5*f* overlap. One such compound is $NpAl_2$, which forms in the cubic Laves phase structure and orders[2] ferromagnetically at 56 °K.

It has been shown by Gossard *et al.*,[3] that UAl_2 (isostructural with $NpAl_2$) does not form local 5*f* or 6*d* moments nor does long-range magnetic order occur. Preliminary measurements[4,5] by the authors on $U_{1-x}Pu_xAl_2$ indicated that magnetic ordering occurs for $x = 0.3$ at 6 °K, whereas $PuAl_2$ is similar magnetically to UAl_2, i.e., no long-range magnetic order. Yet the resistivity-temperature curve for $PuAl_2$ (see Fig. 1) has a remarkable shape for a material without magnetic order. In a recent paper,[6] it was proposed that the resistivity-temperature curve for $PuAl_2$ is dominated at low temperatures by spin fluctuation ($\rho \propto T^2$), and that at higher temperatures a breakdown occurs in the 5*f*-6*d* (or -7*s*) hybridization due to broadening of the 5*f* level.

It is the purpose of this paper to present extensive results on the $U_{1-x}Pu_xAl_2$ system. They include bulk properties—electrical resistivity and magnetic susceptibility—as well as pulsed nuclear magnetic resonance of the common ^{27}Al nucleus. Since the proposed dehybridization in $PuAl_2$ should be a strong function of atomic order in the system, the measurements were repeated on samples which had been disordered by the self-irradiation damage accumulated during storage. The systematic trend of the *s*-*f* hybridization at the Fermi energy as plutonium is substituted for uranium is shown to play a dominant role in the electrical resistivity, Knight shift, and spin-lattice relaxation rate. As the plutonium concentration is increased the virtual bound 5*f* state changes from nonresonant to resonant in behavior until in $PuAl_2$ it becomes coherently hybridized at $T = 0$ °K with the conduction-band states.

In Sec. II we present the experimental procedure. Section III contains a presentation of electrical resistivity, magnetic susceptibility, and nuclear-magnetic-resonance results. The experimental results are discussed in Sec. IV. The conclusions are summarized in Sec. V.

II. EXPERIMENTAL PROCEDURE

A. Sample Preparation

Carefully weighed amounts of the constituent metals (99.99%-pure Al and 99.9%-pure Pu and U) were arc melted together in an argon atmosphere to form buttons of the various alloys. These were turned over and remelted three times to ensure homogeneity. Resistivity specimens measuring $\approx 1.5 \times 1.5 \times 10$ mm were spark cut from the buttons and lightly polished mechanically to remove surface material. No encapsulation was necessary since all resistivity measurements were done in a glovebox.

Approximately 1 g of each alloy was sealed in an aluminum capsule for magnetic susceptibility measurements while an approximately equal amount was powdered (200 mesh) and sealed in an Epoxy capsule for NMR measurements. X-ray powder patterns were obtained for each composition in order to verify that the alloys were single phase. The lattice parameter varied smoothly from 7.811 Å for UAl_2 to 7.831 Å for $PuAl_2$.

B. Electrical Resistivity

The standard four-probe dc method with pressure contacts was used in resistivity (ρ) measurements.

The measuring apparatus and temperature control methods are described elsewhere.[7] Temperature control was better than ± 1 °K, while maximum error in the absolute resistivity was ± 2%. Measurements were made in the range 1.2–300 °K. Both well-annealed (or freshly prepared) specimens and specimens damaged by self-irradiation were studied. Self-irradiation damage in these brittle materials was obtained by merely allowing the specimens to sit for several months at room temperature. Damage thus obtained did not anneal out below room temperature. Self-damage was completely removed by annealing the specimens at 800 °C for 10 h at 10^{-5} Torr. Because of the rapid rate of self-damage, data for annealed specimens had to be obtained within days after the alloy was arc melted or annealed.

C. Magnetic Susceptibility

Magnetic susceptibilities (χ) were measured isothermally by the Faraday method in fields up to 14.5 kOe. Relatively large corrections were needed for the chain and aluminum capsule so that reproducibility was only about $\pm 5\times10^{-8}$ emu/g. Although the effect of damage was less dramatic on χ than on ρ, the same procedure of rapidly obtaining data was followed.

D. Nuclear-Magnetic-Resonance Techniques

The nuclear-magnetic-resonance (NMR) measurements were made at 4, 8, and 12 MHz with a phase-coherent cross-coiled pulsed-NMR spectrometer. A boxcar integrator was used to enhance the signal-to-noise ratio. Radio frequency magnetic fields H_1 of up to about 140 Oe were used. The magnetic field was supplied by a Varian electromagnet with Fieldial control. The ^{27}Al nuclear-resonance profiles were obtained by integrating either the free induction decay (FID) or the echo following a two-pulse sequence. A boxcar gate much greater than the FID time was used while the magnetic field was swept. T_1 measurements were made by saturating the nuclear spin system with a comb of 90° pulses and measuring the recovery of the longitudinal magnetization $M(\tau)$ at a time τ later with a two-pulse sequence. Single-exponential recovery was found in all cases. Below room temperature, T_1 measurements were made by immersing the Epoxy encapsulated powdered samples in various cryogenic liquids.

III. RESULTS

A. Electrical-Resistivity Results

1. Annealed Specimens

The ρ-vs-T curves of the $(U_{1-x}Pu_x)Al_2$ alloys are shown in Fig. 1 for $x=0$ and 1 and in Fig. 2 for $x\neq0$ or 1. For $x=0$ and 1, ρ goes to zero at $T=0$ aside from a residual resistivity term, since the compounds are atomically well ordered. The resistivities of both UAl_2 and $PuAl_2$ vary[6] as T^2 near $T=0$. The large peak and dramatic drop in ρ in $PuAl_2$ is not associated with a magnetic transition as the NMR and χ data clearly show. There is an upturn in the ρ-vs-T curve of $PuAl_2$ at ~270 °K as phonon scattering begins to contribute significantly.

In all compounds above $x=0.1$ a negative $d\rho/dt$ is observed for at least part of the range of temperatures measured (Fig. 2). The decrease in ρ with increasing T is not exponential. For the Pu-rich alloys no minimum is observed up to 300 °K although $d\rho/dt$ is nearly zero at high T. The shallow minimum for $x=0.3$ appears to be a result of an interplay between two anomalous scattering mechanisms.

Kinks are observed in ρ for $x\geq0.7$. The temperatures at which they occur are plotted in Fig. 8 as a function of composition. Kinks or peaks are also observed in χ at these temperatures (see section on χ). For $x=0.5$ a resistivity peak is observed at $T=1.5$ °K.

The addition of $PuAl_2$ to UAl_2 causes minor increases in resistivity at high temperatures, with Mathiessen's rule approximately obeyed. Below ~100 °C, a total breakdown of Mathiessen's rule occurs, particularly at the $PuAl_2$ end of the series. The breakdown of Mathiessen's rule is even more obvious in radiation-damaged samples.

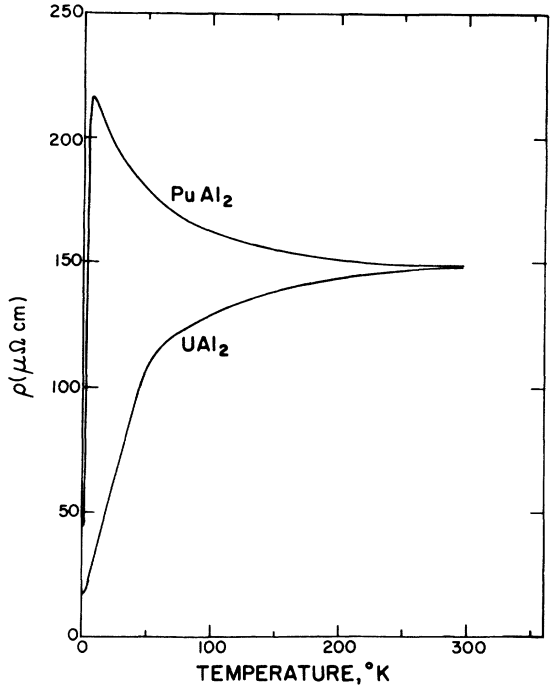

FIG. 1. Resistivities of annealed $PuAl_2$ and UAl_2 as a function of temperature.

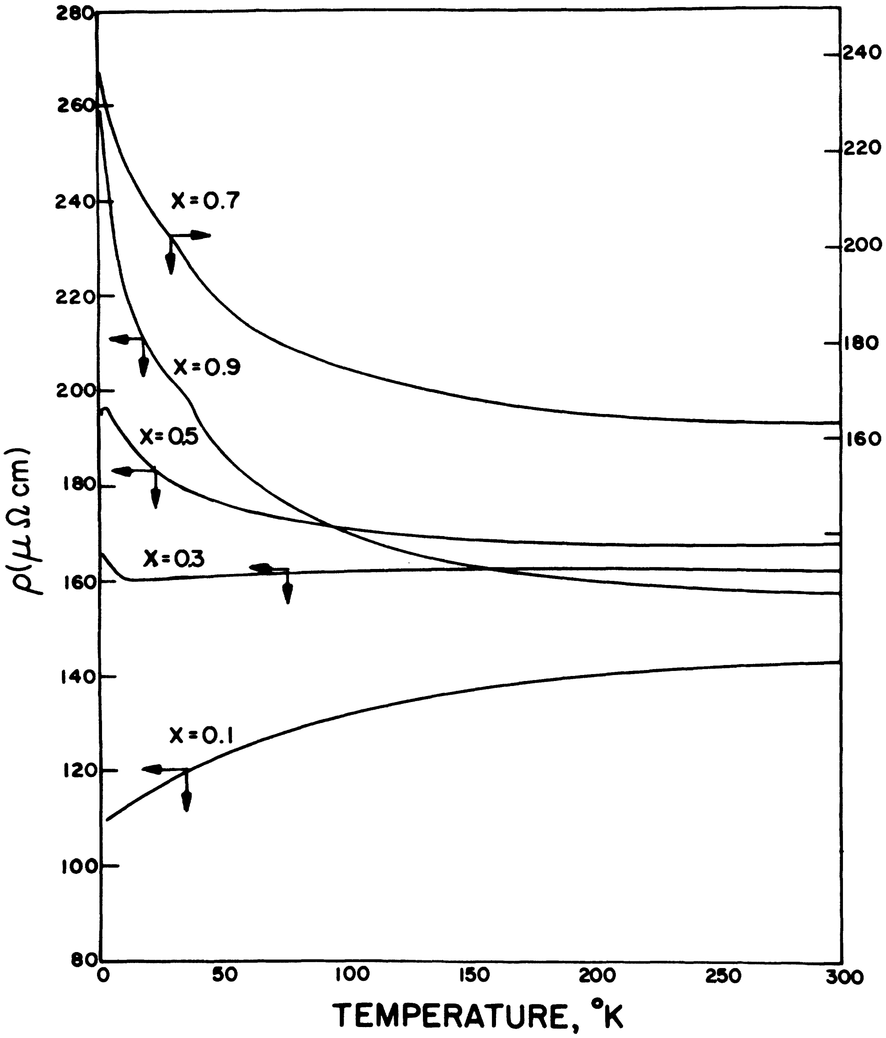

FIG. 2. Resistivities of annealed specimens of $U_{1-x}Pu_xAl_2$ ($x = 0.1$ to 0.9) as a function of temperature. Scale is at right for $x = 0.7$. Note small peak for $x = 0.5$.

2. Self-Damaged Specimens

Resistivities of the self-damaged alloys and compounds are shown in Fig. 3 for $x = 0.1$ to $x = 1.0$ (UAl_2 does not self-damage sufficiently in the time allowed since the half-life of ^{238}U is 4.5×10^9 yr compared to 2.4×10^4 yr for ^{239}Pu). Some specimens were allowed to damage for 3 yr prior to measurement, but it was found that at least in $PuAl_2$, saturation damage is obtained in 3 months. The most dramatic change due to self-damage is observed in $PuAl_2$, where the sharp drop below 8 °K has completely disappeared. In $PuAl_2$ the annealing procedure described above completely removes the self-damage.

Figure 4 is a plot of $\Delta\rho = \rho_{\text{damage}} - \rho_{\text{annealed}}$ in $\mu\Omega$ cm for $x = 0.1$, 0.3, and 0.5. The absolute uncertainty in $\Delta\rho$ is ~1–2 $\mu\Omega$ cm for all curves. It can be seen that radiation damage results in very unusual behavior. While one normally expects the resistivity to increase with damage owing to vacancy and interstitial scattering, we see that in all cases except $x = 0.1$, $\Delta\rho$ is strongly negative and decreases below ~50 °K. For $x = 0.1$ it is negative at high temperatures but positive at low temperatures. Mathiessen's rule would state that $\Delta\rho$ should be positive and roughly constant at all temperatures. Above 150 °K all curves of $\Delta\rho$ are relatively flat. Clearly then, we have two scattering components being affected by radiation damage: (i) a normal atomic disorder scattering term causing a resistivity change $\Delta\rho_1$ which is constant and positive with temperature; and (ii) a term ($\Delta\rho_2$) which is negative, and which (except for $x = 0.1$) decreases far more rapidly at low temperatures than at high temperatures. The scattering associated with $\Delta\rho_2$ is certainly the dominant scattering mechanism. For $x \geq 0.7$ (not shown in Fig. 4), $|\Delta\rho_1| > |\Delta\rho_2|$ above 150 °K.

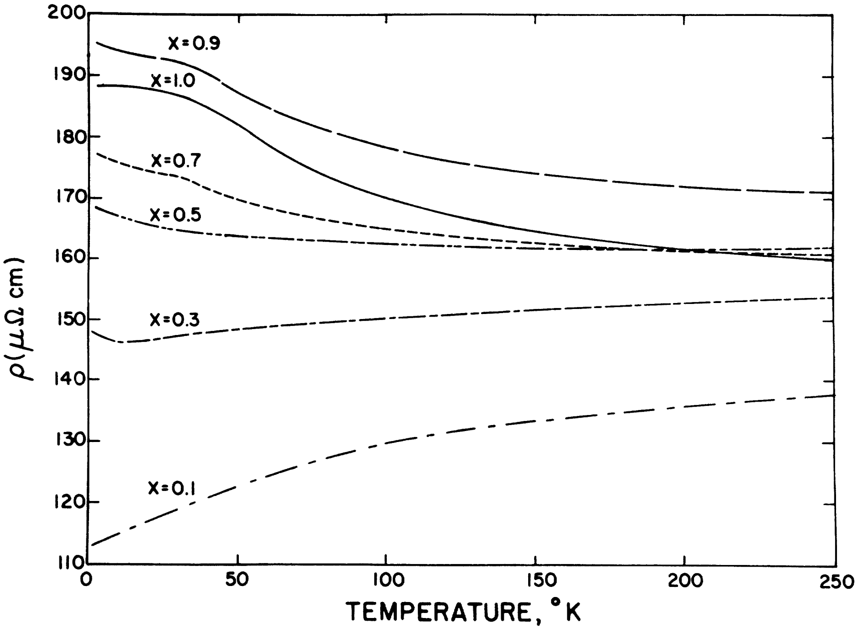

FIG. 3. Resistivity vs temperature of $U_{1-x}Pu_xAl_2$ damaged by self-irradiation. No damage data were obtained for UAl_2.

B. Magnetic-Susceptibility Results

1. Annealed Specimens

Plots of magnetic susceptibility (χ) vs T are shown in Fig. 5. Above ~50 °K all the curves, with the exception of UAl_2, can be fit to the equation

$$\chi - \chi_0 = C/(T-\Theta) \ ,$$

where χ_0 is a constant conduction band term. From the slope C one obtains the effective paramagnetic moment p_{eff}. Table I lists the values of χ_0, P_{eff}, and Θ obtained from a computer fit of the data to the above equation.

Peaks or kinks are observed in χ at low temperatures in all curves at temperatures that roughly correspond to kinks observed in the resistivity (see Fig. 8). (In $PuAl_2$, i.e., for $x=1$, χ merely changes slope at ~40 °K.)

2. Self-Damaged Specimens

Self-radiation damage again causes considerable

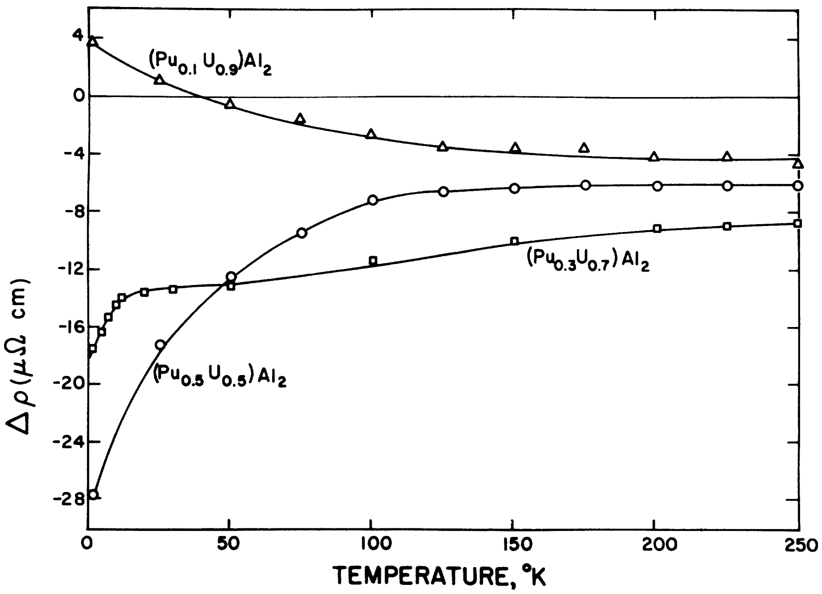

FIG. 4. Plot of $\Delta\rho = \rho_{\mathrm{self\text{-}damaged}} - \rho_{\mathrm{annealed}}$ vs temperature for $x=0.1$, 0.3, and 0.5. For $x>0.5$, $\Delta\rho$ is qualitatively similar to that of $x=0.5$. Note that for $x=0.1$ the curvature is of opposite sign from that of the other curves.

TABLE I. Parameters obtained in fitting χ above the peaks to the equation $\chi - \chi_0 = C/(T - \Theta)$.

Compound	χ_0 in 10^{-6} emu/g^{-1}	$P_{eff} \pm 0.1$ per actinide	per Pu atom	Θ, °K	Location of kink or peak, in χ, °K
$x = 0$ (UAl$_2$)	0 ± 0.2	...	...	...	...
$x = 0.1$	0	3.0	9.3	−208	...
$x = 0.3$	1.6	2.0	3.7	−72	6
$x = 0.5$	1.4	1.8	2.5	−50	15
$x = 0.7$	1.3	1.4	1.7	−35	20
$x = 0.9$	1.2	1.0	1.1	−30	34
$x = 1.0$ (PuAl$_2$)	0.5	1.1	1.1	−150	40

changes in χ, primarily for $x \lesssim 0.7$. The curves are shown in Fig. 6. While in most cases the damage results in either a smearing out or elimination of peaks or kinks in χ, we find that for $x = 0.3$ damage results in a large exaggeration of the peak at 6 °K. This is the composition for which the NMR signal disappears at 6 °K, indicating magnetic ordering.

For $x > 0.3$ the peaks in χ generally disappear after damage. In the damaged samples the initial variation of χ with temperatures goes as $\chi_0(1 - CT^n)$ near $T = 0$. In the Pu-rich alloys n generally equals ~2.0 (Fig. 7). For $x = 0.9$ (not shown), n~2.2.

C. Nuclear-Magnetic-Resonance Results

1. *Absorption Spectra*

The resonance spectra for the cubic Laves-phases U$_{1-x}$Pu$_x$Al$_2$ compounds fall into two categories (see Fig. 8): those that have essentially no magnetic broadening and do not form a magnetic echo following a $\frac{1}{2}\pi$-π pulse sequence, and those that are broadened magnetically and do have a magnetic echo.

a. No magnetic broadening. The spectra for UAl$_2$ at 4.2 °K (Figs. 9 and 10) are quite ideal powder patterns exhibiting first- and second-order quadrupole broadening and small anisotropic Knight shift. Second-order quadrupole shifts of the satellites are distinguishable. Also shown in Figs. 9 and 10 are the computer-generated synthetic powder patterns.[8] Table II lists the values of the mean electric field gradient (efg) q_0, the fractional width of the efg distribution $\Delta q/q_0$, the axial Knight shift K_{ax}, and the second moment $\langle \Delta\nu_D^2 \rangle_{av}^{1/2}$ of the unperturbed Gaussian resonance line used in the convolution. The parameters are those that best fit the spectra for all the compounds at 77 °K. Here $\Delta q/q_0 = 2\langle \Delta q^2 \rangle^{1/2}/q_0$. That is $\Delta q/q_0 = 1.7$ times the half-width-at-half-maximum intensity of a Gaussian distribution of efg's.

The spectra for PuAl$_2$ at 77 °K (see Figs. 11 and 12) exhibit a marked dependence on sample history due to the self-radiation damage caused by the decay of ^{239}Pu. Also exhibited in Figs. 11 and 12 are the computer-generated powder patterns for the central transition. It is interesting to note that the spectra of the damaged PuAl$_2$ (Fig. 12) is not described by a Gaussian distribution of electric field gradients, but, in fact must have a significant component at the zero value of efg. It appears, that in addition to a random disordering of the lattice due to radiation damage, there is a greater than random probability for an aluminum atom to sit in a cubic environment. One way this could occur is by displacement of an aluminum atom to a plutonium site.

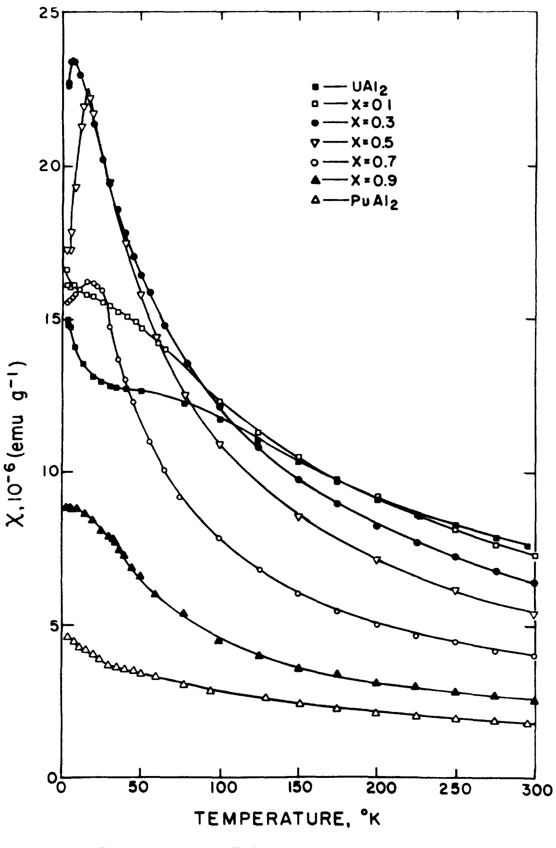

FIG. 5. χ vs T for annealed U$_{1-x}$Pu$_x$Al$_2$.

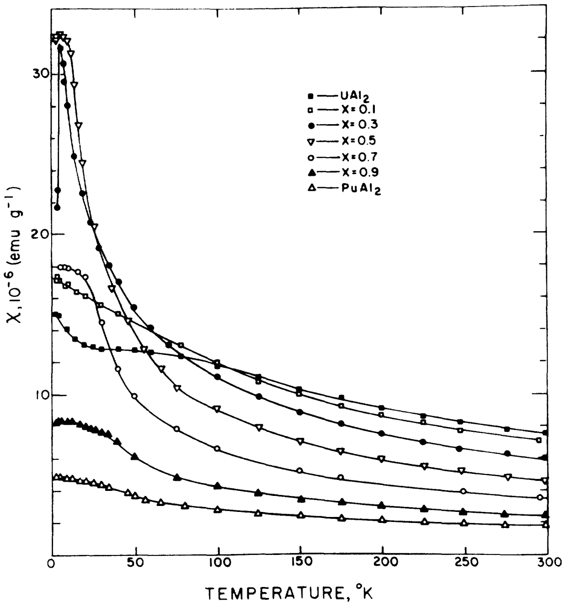

FIG. 6. χ vs T for self-irradiation damaged specimens of $U_{1-x}Pu_xAl_2$.

The plutonium sites have cubic point symmetry.

The intermediate compositions between UAl_2 and $PuAl_2$ show broadening due to a distribution of efg's resulting from the chemical disordering on the actinide sublattice. The 77 °K spectra can, however, be fit rather well by a Gaussian distribution of efg's. The parameters in the computer fits are given in Table II. From the values of $\Delta q/q_0$, we see there is *no* apparent tendency for chemical ordering near the $x=0.5$ composition.

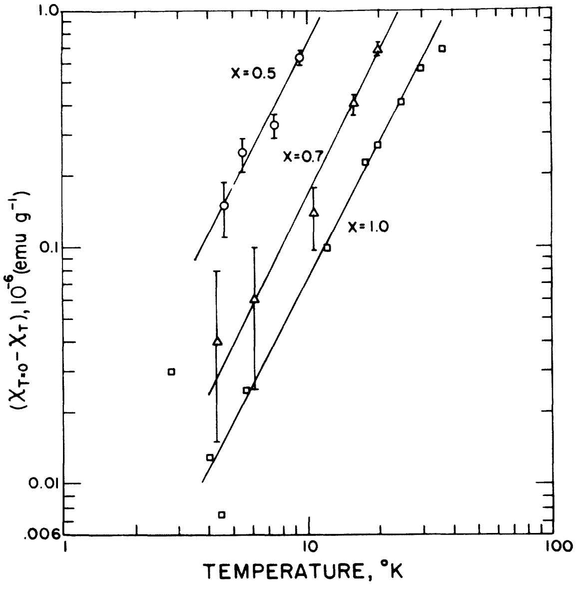

FIG. 7. Log-log plot of magnetic susceptibility vs temperature of three compositions of damaged $U_{1-x}Pu_xAl_2$. The susceptibility at $T=0$ has been subtracted. Straight lines correspond to a slope of 2.0. For $x=0.9$ (not shown) slope is 2.2.

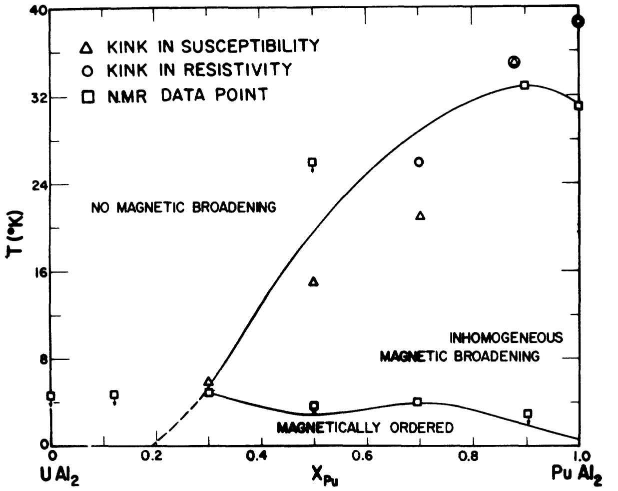

FIG. 8. Magnetic phase diagram of $U_{1-x}Pu_xAl_2$. See text for description of different regimes and measurements.

For all the compounds the Knight shift K is linear in the susceptibility χ.[5] In Table III the slope α of the K-vs-χ curve as well as the intercept $\chi(K=0)$ is given as a function of composition. We have also listed χ_{orb}, the second-order Van Vleck temperature-independent susceptibility, obtained in the manner of Gossard *et al.*[3] It is clear that $\chi(K=0)$ and χ_{orb} have the same qualitative composition dependence, and thus the uncertainties in determining χ_{orb} from $\chi(K=0)$ need not concern us here.

b. Magnetically broadened. Referring to Fig. 8, the spectra broaden smoothly with decreasing temperature in the temperature range marked "magnetic broadening." The onset of magnetic order has been found in the two samples of $U_{0.7}Pu_{0.3}Al_2$ measured at approximately 6 °K and in one of the two samples of $U_{0.3}Pu_{0.7}Al_2$ measured at approximately 4 °K. The onset of magnetic order is observed by the sudden disappearance of the resonance signal upon cooling. In Fig. 13 the resonance patterns of $U_{0.7}Pu_{0.3}Al_2$ at 7 and 6 °K are shown. The computer fit to the spectra at 7 °K requires a small amount of magnetic broadening corresponding to a Gaussian line shape with second moment of $(45\text{ kHz})^2$, i.e., $(37\text{ Oe})^2$.

Magnetic broadening approaching a magnetic transition is not unusual for a chemically inhomogeneous system such as the disordered compounds with $0.3 \leq x \leq 1$, where the aluminum nuclei have a distribution of internal magnetic fields. However, for $PuAl_2$ where the high-temperature spectra show

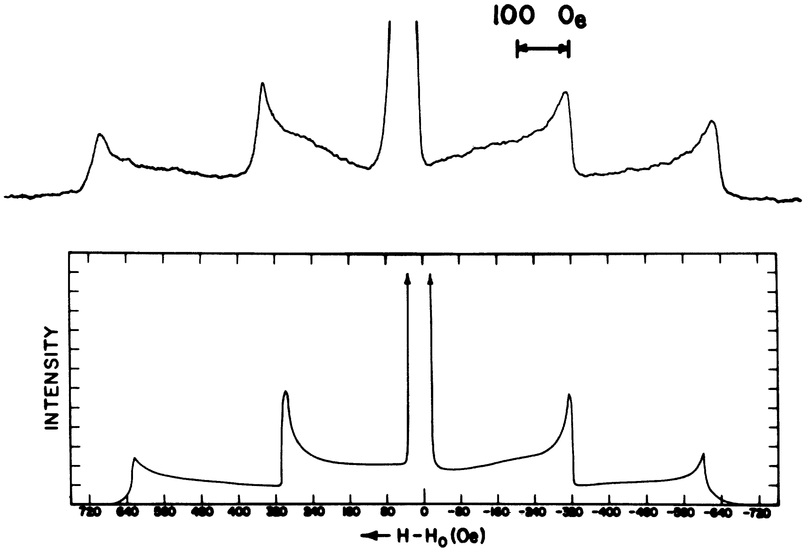

FIG. 9. (Top) Experimental Fourier transform (see text) of PNMR quadrupole echo for UAl_2 at 4.2 °K and 12 MHz. Magnetic field increases to the left. Data obtained with a repetition time of 160 msec, a boxcar gate of 160 μsec, and a time constant of 10 msec. Central transition truncated. (Bottom) Synthetic powder pattern obtained with $\langle\Delta\nu_D^2\rangle^{1/2} = 3.5$ kHz, $q_0 = 0.89 \times 10^{24}$ cm^{-3}, and $K_{ax} = +2.0 \times 10^{-4}$. Central transition truncated.

a well-ordered compound, we find linewidths approaching 1000 G at low temperature. In Fig. 14, we display the temperature dependence of the linewidth for $PuAl_2$ at 12 MHz. Also plotted is a Curie-Weiss-type plot of the reciprocal linewidth, where the residual ~ 50-G linewidth is that due to the second-order quadrupole broadening of the central transition at 77 °K. Note that in UAl_2 and $U_{0.9}Pu_{0.1}Al_2$ no magnetic broadening is found down to ~ 2 °K.

It is important to note that the spin phase-coherence time T_2, (the rate of decay of the Hahn echo as a function of pulse separation), measured in the temperature regime of extreme magnetic broadening is comparable to its value at temperatures of 77 °K and above and is at least one order of magnitude longer than the inverse linewidth. This indicates that the broadening is due to an inhomogeneous magnetic interaction and not due to lifetime effects.

2. Spin-lattice Relaxation

In Table II we list the value of T_1T for the ^{27}Al nucleus at 77 °K for all compositions studied. The temperature dependence for T_1T for UAl_2 and $PuAl_2$ has been reported.[9] Whereas for UAl_2 we find no simple dependence of $(T_1T)^{-1}$ on susceptibility χ, for $PuAl_2$ we find a quadratic dependence of $(T_1T)^{-1}$ on χ. No field dependence of $(T_1T)^{-1}$ has been found between ~ 3.6 and 10.8 kOe.

IV. DISCUSSION

A. Electrical Resistivity and Magnetic Susceptibility

In order to understand the ternary system $(U_{1-x}Pu_x)Al_2$, our attention must first focus on the end points which we have already considered in a previous paper. As stated, we have attributed[6] the T^2 behavior of the resistivity at low temperatures

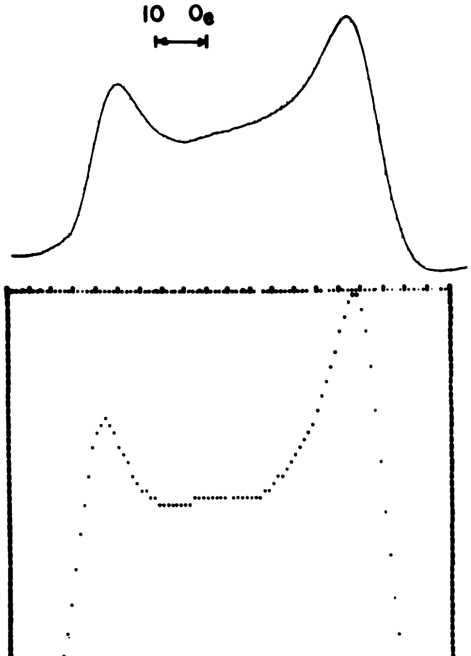

FIG. 10. (Top) Experimental Fourier transform (see text) of PNMR free induction decay for UAl_2 at 4.2 °K and 12 MHz. Central transition only. Magnetic field increases to the right. Data obtained with a repetition time of 120 msec, a boxcar gate of 160 μsec, and a time constant of 10 msec. (Bottom) Synthetic powder pattern obtained with the same parameters as in Fig. 9. Central transition only. Major division on field axis is 3.8 Oe.

TABLE II. Resonance parameters for $U_{1-x}Pu_xAl_2$ at 77 °K.

X	0.0	0.1	0.3	0.5	0.7	0.9	1.0
$q_0(10^{24}\ \mathrm{cm}^{-3})$[a]	0.91	0.92	0.93	0.85	0.80	0.72	0.73
$\Delta q/q_0$	0.00	0.15	0.25	0.30	0.20	0.10	0.00
$K_{\mathrm{ax}}(10^{-4})$	+1.0	~0	~0	~0	~0	~0	−2.0
$(\Delta\nu_D^2)_{\mathrm{av}}^{1/2}$ (kHz)	3.5	~3.4	~3.3	~3.1	~3.1	~3.1	3.0
$(T_1T)^{-1}$ (sec °K)$^{-1}$	1.18	1.96	2.85	4.20	4.46	6.67	7.14
$K_{\mathrm{iso}}(10^{-2})$[b]	0.82	0.92	0.92	1.07	0.93	0.62	0.58

[a] Nuclear electric quadrupole moment of ^{27}Al is 0.149×10^{-24} cm^2.

[b] Knight shifts are referred to the gyromagnetic ratio $\gamma=11.094$ MHz/10 kOe.

to spin-flip scattering of conduction electrons from localized spin fluctuations (lsf) in the narrow f bands in both UAl_2 and $PuAl_2$. At slightly elevated temperatures it is necessary to invoke spin-fluctuation-induced dehybridization of f bands to understand the resistivity of $PuAl_2$. The ternary system $(U_{1-x}Pu_x)Al_2$ then shows us a progression of behavior from resonant to nonresonant scattering as we go from $PuAl_2$ to UAl_2.

A brief summary of the behavior expected in resistivity and magnetic susceptibility in both alloys and well-ordered intermetallic compounds in the presence of lsf is in order here. Kaiser and Doniach[10] have shown for the case of dilute alloys that for $T \ll T_S$ (the characteristic temperature corresponding to the maximum in the lsf spectral density), two cases must be distinguished: (i) a resonant case where the Fermi level lies in the middle of a virtual bound f state and potential scattering is at a maximum, and (ii) an off-resonance case where the Fermi level is not near the middle of the f state and there is little or no potential scattering. At $T=0$ there is no scattering from lsf since the spectral density is zero. The lsf contribution to the scattering rate $1/\tau$ varies as T^2 for small T. For the resonant case this additional scattering broadens the f state, pushing it off the resonance so that $1/\tau \propto 1/\tau_1(1-AT^2)$. For case ii, Kaiser and Doniach show that $1/\tau \propto 1/\tau_2(1+BT^2)$. Similarly, the magnetic susceptibility χ either varies as $(1-CT^2)$ for case i, or flattens out below T_S for case ii. Above T_S, a Curie-Weiss behavior for χ is expected.

For atomically ordered compounds the energy bands in the one-electron picture are well defined near $T=0$ and a well-defined Fermi surface is formed. Thus, $1/\tau \rightarrow 0$ apart from a small residual resistivity. Doniach[11,12] shows that for $0<T\ll T_S$, one expects $1/\tau \propto T^2$ and for $T \lesssim T_S$, $1/\tau \propto T$. Above T_S the resistivity may flatten out or even decrease as the mean free path of the f-band electrons approaches the interatomic spacing.

As pointed out, UAl_2 appears to be dominated by spin-fluctuation scattering. Near $T=0$, the resistivity first varies as T^2 and then follows the pattern predicted by Doniach[12] for materials where no dehybridization occurs. Since χ flattens out near $T=80$ °K, then, based on Doniach's model, $T_S \approx 80$ °K.

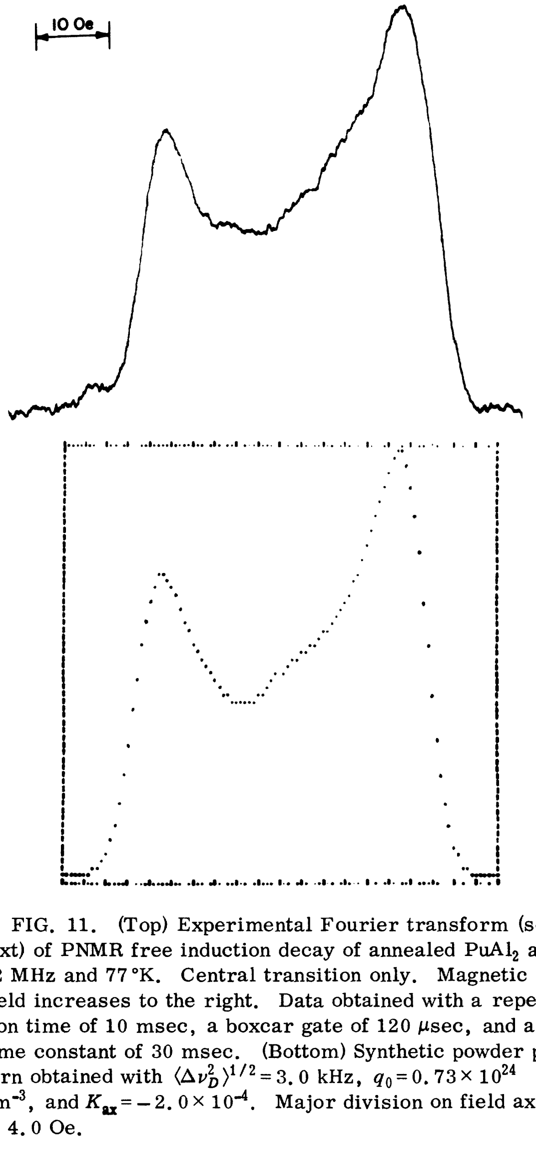

FIG. 11. (Top) Experimental Fourier transform (see text) of PNMR free induction decay of annealed $PuAl_2$ at 12 MHz and 77 °K. Central transition only. Magnetic field increases to the right. Data obtained with a repetition time of 10 msec, a boxcar gate of 120 μsec, and a time constant of 30 msec. (Bottom) Synthetic powder pattern obtained with $\langle\Delta\nu_D^2\rangle^{1/2}=3.0$ kHz, $q_0=0.73\times10^{24}$ cm^{-3}, and $K_{\mathrm{ax}}=-2.0\times10^{-4}$. Major division on field axis is 4.0 Oe.

TABLE III. Resonance results for $U_{1-x}Pu_xAl_2$.

	0.0	0.1	0.3	0.5	0.7	0.9	1.0
$q_0 a_0^3$ [a]	426	432	439	404	383	347	353
$\Delta q_{1/2} a_0^3$ [b]	0.0	38	65	71	45	20	0.0
α (emu/mole)$^{-1}$	2.9(2)	2.7(2)	3.3(3)	3.8(2)	5.0(2)	5.1(5)	11.2(4)
$\chi(0)$ (10^{-4} emu/mole)	7 (2)	6 (2)	9 (2)	8 (1)	8 (1)	4 (1)	4 (1)
χ_{orb} (10^{-4} emu/mole)	10	9	11	10	9	5	4
$K_{iso}^2 T_1 T/S$ [c]	14.7	11.1	7.71	6.94	4.88	1.47	1.23

[a] q_0 from 77 °K resonance data, a_0 from room-temperature x-ray powder patterns.
[b] Half-width at half-maximum intensity of a Gaussian distribution of efg's.
[c] 77 °K results; S is the Korringa constant equal to $(\gamma_e/\gamma_n)^2(\hbar/4\pi k_B)$.

The $PuAl_2$ resistivity, however, can be fit (see Ref. 6) between 1 and 4 °K to the equation

$$\rho = \rho_0 + AT^2 + Be^{-\theta/T} \quad , \tag{1}$$

where ρ_0, A, E, and θ are constants. The exponential term becomes dominant by 2 °K, indicating a scattering process in addition to spin fluctuations. While the functional form for the process of dehybridization is not yet known it appears likely that the exponential term is associated with this process. Experimental evidence for dehybridization is obtained from ρ and χ of self-irradiation damaged $PuAl_2$. Both these properties vary as $(1 - T^2)$ near $T = 0$ for the damaged $PuAl_2$, indicating that the f states have formed virtual-bound levels centered very nearly at the Fermi energy thus giving rise to resonant potential scattering. The damaged compound is now behaving as a disordered alloy. Since the damaged and well-ordered material behave nearly identically above ~30 °K, we conclude that the coherence of the hybridized band states in the well ordered compound has been destroyed for $T \gtrsim 30$ °K, and resonant scattering from virtual-bound states is dominant. The negative slope of the ρ-vs-T curve is a consequence of additional spin-fluctuation broadening of the f levels which are then pushed off resonance.

Doniach[12] argues that the dehybridization effect itself is spin-fluctuation induced in the well-ordered compound. He assumes a T^2 law for the broadening of the f levels by the spin fluctuations:

$$\Gamma_f = A(T/T_S)^2 \quad . \tag{2}$$

As Γ_f increases to become comparable with $(E_F - \epsilon_f)$ (where E_F is the Fermi level and ϵ_f is the center of the unhybridized f level), the depression in the density of states formed by the hybridization begins to fill. The effect is to pull the Fermi level toward ϵ_f. Since $1/\tau$ is given by

$$\frac{1}{\tau} = \mathrm{Im}\,\frac{v_{kf}^2}{E_F - \epsilon_f - i\Gamma_f} \quad , \tag{3}$$

where v_{kf} is the hybridization energy, Doniach points out that as $(E_F - \epsilon_f)$ becomes small compared to Γ_f, $1/\tau$ is given by

$$1/\tau = v_{kf}^2/\Gamma_f \quad , \tag{4}$$

which is just the resonance-scattering value obtained by Kaiser and Doniach[10] for dilute alloys.

As UAl_2 is added to $PuAl_2$ we create essentially

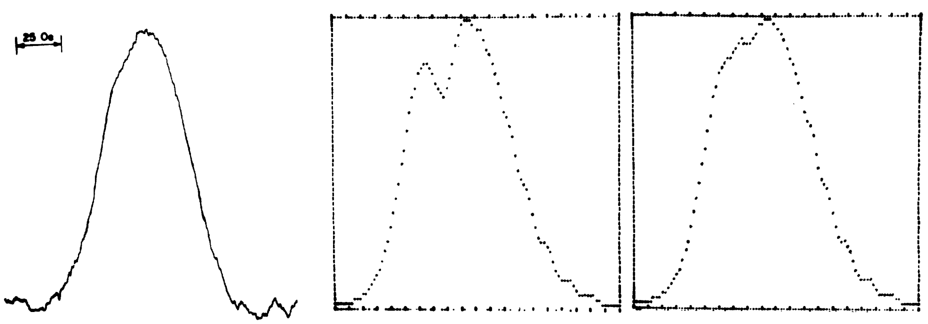

FIG. 12. (Left) Experimental Fourier transform (see text) of PNMR free induction decay of damaged $PuAl_2$. Experimental parameters identical to those in Fig. 11. Magnetic field increases to the right. (Middle) Synthetic power pattern obtained with $\langle \Delta\nu_D^2 \rangle^{1/2} = 3.0$ kHz. $q_0 = 0.87 \times 10^{24}$ cm^{-3}, $K_{ax} = -2 \times 10^{-4}$, and $\Delta q/q_0 = 0.5$. (Right) Same as (middle) but with an additional component with $q = 0$ and relative weight of 0.03. Major division on horizontal axis is 6.6 Oe.

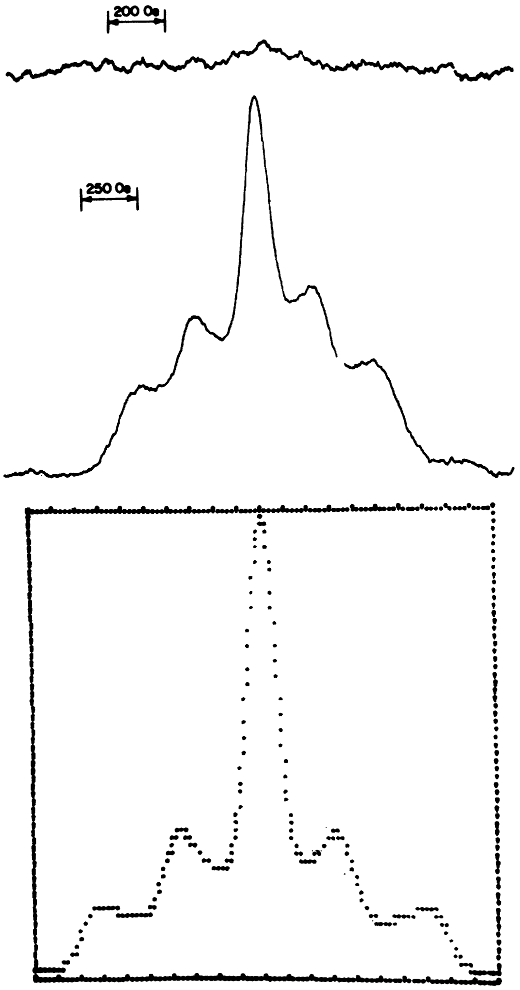

FIG. 13. Experimental Fourier transform (see text) of PNMR magnetic echo for $U_{0.7}Pu_{0.3}Al_2$. Magnetic field increases to the right. (Top) $T - T_N \simeq 0$ °K (middle) $T - T_N \simeq 1$ °K. Data obtained with a repetition time of 40 msec, a boxcar gate of 20 μsec, and a time constant of 10 msec. (Bottom) Synthetic power pattern obtained with $\langle \Delta\nu^2 \rangle^{1/2} = 45$ kHz, $q_0 = 0.82 \times 10^{24}$ cm^{-3}, and $K_{ax} = 0$. Major division on field axis 73.8 Oe.

a disordered alloy so that a well-defined Fermi surface is not formed and the f bands remain as virtual-bound states down to the lowest temperatures. The resistivity at $T = 0$ therefore remains large. For $x = 0.9$ and 0.7 the f levels probably remain very nearly centered around E_F since the resonant potential scattering is undiminished ($\rho_{PuAl_2} - \rho_{alloy}$ is reasonably constant above 10 °K for both these alloys).

For values of $x \leq 0.5$ there is a definite shift of ϵ_f relative to E_F since the low-temperature scattering begins to drop drastically. For $x = 0.3$ the f level has shifted sufficiently that only a trace of resonant potential scattering remains, while for $x = 0.1$ there is no longer any evidence for it. This result is consistent with the small degree of hybridization in UAl_2 (see discussion for NMR results) where the f band is centered away from the Fermi level.

The damaged specimens show a tendency toward saturation in ρ near $T = 0$ for $x \geq 0.7$. Further, the saturation value of the resistivity is in each case considerably lower (10–20%) than the peak value of the annealed specimens. A $(1 - T^2)$ variation is also observed in the magnetic susceptibility for these same alloys near $T = 0$ (Figs. 6 and 7). These results can be understood in terms of Eqs. (2)–(4) by assuming that in the damaged state the broadening of the f levels is a combination of a spin-fluctuation term plus a constant term resulting from lattice disorder and lattice expansion, i.e.,

$$\Gamma_f = A + B(T/T_S)^2 \ . \qquad (5)$$

Because of lattice expansion the quantity $(E_F - \epsilon_f)$ may also change somewhat with damage. In any event we can see from Eq. (4) that the existence of a scattering term due to lattice disorder will decrease $1/\tau$ at the lowest temperatures. For very small T this term is likely to be much larger than the T^2 term, hence the approach to saturation. It does not seem necessary to assume a change in T_S to describe the data of damaged specimens.

For $x = 0$ and 0.1 the f level is off resonance so

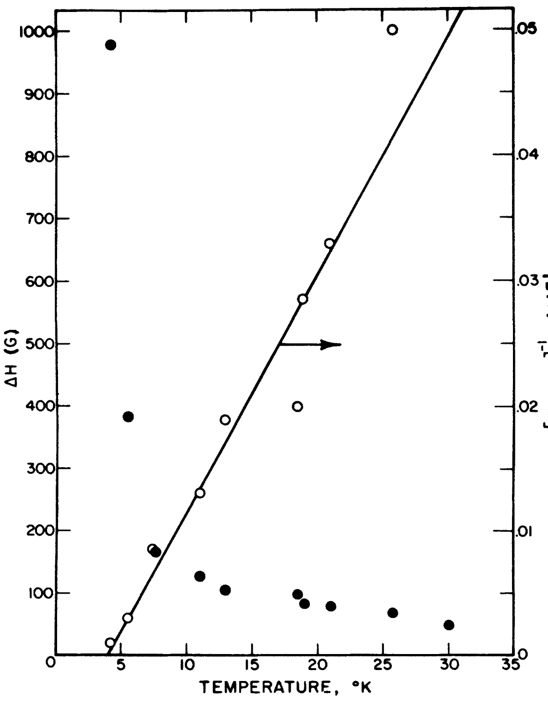

FIG. 14. Linewidth and reciprocal excess linewidth vs temperature for $PuAl_2$ at 12 MHz.

that any scattering in addition to spin fluctuations can only increase the resistivity near $T=0$. Figure 4 shows $\Delta\rho = (\rho_{\text{damaged}} - \rho_{\text{annealed}})$ for $x=0.1$ to 0.5. It is obvious that vacancy and interstitial scattering indeed gives a positive contribution to ρ near $T=0$ for $x=0.1$. It is expected that a similar result would be obtained for UAl_2. An experiment is planned to bombard UAl_2 with neutrons to obtain a damaged specimen.

In the damaged samples, at high temperatures, there are at least two competing contributions to $\Delta\rho$: (i) a lattice disorder term (vacancy, interstitial, and substitutional scattering) which is positive, and (ii) a negative temperature-dependent term resulting from a decrease in spin-fluctuation scattering due to damage. The second term comes about because the competition between local and itinerant behavior in the actinides is critically dependent on the distance between actinide atoms. If a Pu atom, for example, displaces an Al atom, the Pu-Pu distances in its vicinity are decreased leading to greater f-f overlap and an increase in spin-fluctuation temperature. If we assume that at high temperatures the resistivity is primarily due to lsf scattering, then for $U_{0.9}Pu_{0.1}Al_2$ the decrease represents ~4% of the resistivity. Thus something less than 2% of the actinide atoms (we assume that each misplaced actinide atom reduces the magnetism on at least two actinide sites) must sit on aluminum sites in the damaged state, a result not inconsistent with NMR data. For alloys where resonant scattering occurs the situation is more complex and does not lend itself to analysis.

Some features of the data remain unexplained. In particular, kinks in the resistivities of annealed specimens are observed roughly corresponding in temperature to kinks or peaks in magnetic susceptibility and onsets of magnetic broadening in the NMR spectra. In the damaged state these kinks appear to be associated with the onset of $(1-T^2)$ behavior of both resistivity and susceptibility.

B. Nuclear Magnetic Resonance

1. Electric Field Gradient

In Table III we list the values of the efg's at 77 °K multiplied by the cube of the lattice parameter determined at room temperature. (For a detailed discussion of electric field gradients in metals, see Cohen and Reif,[13] Langer and Vosko,[14] Watson *et al.*,[15] and Watson and Freeman.[16]) Also listed are the half-widths at half-maximum $\Delta q_{1/2}$ of the assumed Gaussian distribution of efg's used to fit the spectra. Barnes *et al.*[17] have calculated the point-charge contribution to the efg at the B site in the C-15 structure. Defining $\eta_{\text{latt}} \equiv q_{\text{latt}} a_0^3$, they find

$$\eta_{\text{latt}} = Z_A(-53.775) + Z_B(115.62) \quad . \tag{6}$$

Here Z_A and Z_B are the effective point charges at the A sites and B sites, respectively. The assignment of point charges or alternatively valencies in a metal is quite difficult. The A-site contribution to the field gradient is given to approximately 1% by the first two shells of A atoms with multiplicity 6 and 5, respectively. The B-site contribution to η_{latt} is given to approximately 2% by the first two shells of B atoms with multiplicity 6 and 12, respectively.

Following the treatment of Watson, Gossard, and Yafet[15] (WGY), we write the measured efg as

$$q = (1-\gamma_\infty)\, q_{\text{latt}} + (1-R_Q)\, q' \quad , \tag{7}$$

where $(1-\gamma_\infty)$ and $(1-R_Q)$ are the Sternheimer antishielding and shielding factors, respectively; q_{latt} is the point-charge contribution; and q' is a local field gradient caused by the redistribution of occupied conduction electron states near the Fermi surface. (We neglect q_0 and q'' of WGY that arise from nonspherical potential and orbital distortion, respectively.) The reader is referred to the paper by WGY[15] for detailed discussion of q'. Briefly, q' is the shielding response of the conduction electrons within the spherical potential of the augmented-plane-wave (APW) sphere to the external potential imposed by the field gradient of point charges. It is therefore linear in $-q_{\text{latt}}$ and related to the densities of states at the Fermi level for the various bands. Using this oversimplified approach, we write for the total field gradient multiplied by a_0^3,

$$\eta = (1-\gamma_\infty)\,\eta_{\text{latt}} + (1-R_Q)\,\eta_{\text{latt}}\,\beta\, G^p_{\text{Al}}(E_F) \quad . \tag{8}$$

Here β is a product of an orbital symmetry factor α and the radial integrals $\langle r^2\rangle\langle r^{-3}\rangle$ at the aluminum site, and $G^p_{\text{Al}}(E_F)$ is the p projection (strictly speaking non-s-projection) of the density of states at the Fermi level at the aluminum site. Taking[18] $(1-\gamma_\infty)=3.36$, $(1-R_Q)\simeq 1$, $\langle r^2\rangle\langle r^{-3}\rangle = 39.66\times 10^8$ cm^{-1} from Herman and Skillman[19] $3p^1$ Al atomic wave functions, $\alpha = 0.064$ for spherical p bands,[15] and assuming $\eta < 0$ we find the values of $G^p_{\text{Al}}(E_F)$ shown in Table IV for rare-earth and actinide dialuminides.

Note the use in Table IV of the valence +3 for the rare-earth ions and +4 for the actinide ions. The aluminum valence is taken +3 in both cases. The assignment of the +4 valence for the actinide ions is an arbitrary one but leads to reasonable results. The valence assignment is merely an attempt to estimate the average amount of charge virtually localized on the ion. Focusing on the rare earths[17,20,21] we see rather constant values of $G^p_{\text{Al}}(E_F)$. The small decrease of $G^p_{\text{Al}}(E_F)$ from La through Lu may reflect the diminished $4f$-electron character in the conduction band as one goes across the rare-earth series. For the actinides, the

TABLE IV. Electric field gradients in rare-earth and actinide dialuminides, $A\text{Al}_2$.

A	e^2qQ/h (MHz)	qa_0^3	Z_A	$G_{\text{Al}}^p(E_F)$ States/eV atom
Y	3.97[a]	372	+3	0.147
La	4.63[b]	483	+3	0.163
Ce	4.72[a]	477	+3	0.162
Pr	4.60[c]	459	+3	0.160
Nd	4.56[a]	451	+3	0.158
Er	3.56[a]	326	+3	0.140
Tm	3.45[a]	314	+3	0.138
Yb	2.30[b]	217	+3/+2	0.124/0.117
Lu	2.85[a]	255	+3	0.130
U	4.71	426	+4	0.180
$\text{U}_{0.9}\text{Pu}_{0.1}$	4.77	432	+4	0.182
$\text{U}_{0.7}\text{Pu}_{0.3}$	4.82	439	+4	0.183
$\text{U}_{0.5}\text{Pu}_{0.5}$	4.40	404	+4	0.176
$\text{U}_{0.3}\text{Pu}_{0.7}$	4.14	383	+4	0.171
$\text{U}_{0.1}\text{Pu}_{0.9}$	3.73	347	+4	0.164
Pu	3.78	353	+4	0.165

[a] Barnes and Lecander (Ref. 17).

[b] Jaccarino *et al.* (Ref. 20).

[c] Jones *et al.* (Ref. 21).

range of $|qa_0^3|$ falls between that of Nd and Er, yet we expect a greater $5f$ character in the conduction band for U than the $4f$ character found for Nd. Thus, we suggest the +4 valence is more appropriate for the actinide ions. This assignment leads to values of $G_{\text{Al}}^p(E_F)$ somewhat larger than found in the analogous early rare earths. The narrow range of qa_0^3 for the $\text{U}_{1-x}\text{Pu}_x\text{Al}_2$ compounds is consistent with a nearly equal point-charge assignment for the uranium and plutonium ions.

The broad widths of the efg distribution at intermediate values of X are larger than calculated from a simple distribution of uranium and plutonium on the A sublattice. Consideration of the individual terms in the point charge calculation of q_{latt} leads to the conclusion that near $x = 0.5$ a few percent (~5%) of the ions may in fact be on the wrong sublattice. In the C-15 structure the ratio of atomic radii to the coordination 12 radii suggests that the interchange of atoms to the wrong sublattice is possible. Also, some residual radiation damage may be present in these intermediate compositions.

2. *Knight Shift and Spin-Lattice Relaxation*

The values of $\alpha \equiv dK/d\chi$ shown in Table V have a very strong composition dependence on the Pu-rich side. We will assume that at each composition α is the sum of two contributions

$$\alpha = \alpha_{\text{ex}} + \alpha_{\text{hyb}} \quad . \tag{9}$$

Here α_{ex} is the indirect or effective interband exchange contribution[22] (quantum-mechanical exchange and weak interband mixing) relying on the contact interaction of the conduction electrons at the Fermi energy with the nucleus. α_{hyb} is the re-

TABLE V. Spin polarization at ^{27}Al in A Al_2.

	α_{ex} (G^2/erg)	α_{hyb} (G^2/erg)	$H_{\text{eff}}^{\text{ex}}$ [a] (kOe)	g_J [b]	J_{sf} [c] (eV)	$H_{\text{eff}}^{\text{hyb}}$ [d] (kOe)	f_s [e] (10^{-2})	$H_{\text{eff}}^{\text{hyb}}$/hfs ($10^{-2}$)
Ge	0.84	0.0	−28	6/7	−0.07	+110.0		
Pr	0.94	0.0	−21	4/5	−0.05	0.0		
Nd	1.07	0.0	−16	8/11	−0.04	0.0		
Gd	−1.16	0.0	−13	2	−0.03	0.0		
Tb	−0.72	0.0	−12	3/2	−0.03	0.0		
Dy	−0.49	0.0	−11	4/3	−0.03	0.0		
Ho	−0.57	0.0	−16	5/4	−0.04	0.0		
Er	−0.39	0.0	−13	6/5	−0.03	0.0		
Tm	−0.31	0.0	−12	7/6	−0.03	0.0		
U	+2.9	0.0	+32	2	+0.08	0.0	0.0	0.0
$\text{U}_{0.9}\text{Pu}_{0.1}$	+2.7	0.0	+30	2	+0.08	0.0	0.0	0.0
$\text{U}_{0.7}\text{Pu}_{0.3}$	+2.4	+0.9	+27	2	+0.07	+10	0.96	2.2
$\text{U}_{0.5}\text{Pu}_{0.5}$	+2.1	+1.7	+23	2	+0.06	+19	2.11	4.2
$\text{U}_{0.3}\text{Pu}_{0.7}$	+1.8	+3.2	+20	2	+0.05	+36	4.53	8.0
$\text{U}_{0.1}\text{Pu}_{0.9}$	+1.5	+3.6	+17	2	+0.04	+40	5.63	8.9
Pu	+1.3	+9.9	+15	2	+0.04	+111	16.44	24.7

[a] $H_{\text{eff}}^{\text{ex}} = [g_J/(g_J - 1)]N\mu_B\alpha_{\text{ex}}$. Rare-earth values from Jones (Ref. 24).

[b] Russell-Saunders values assumed for the rare-earth ions; spin-only value assumed for the actinides.

[c] $H_{\text{eff}}^{\text{ex}} = 2H_{\text{hfs}}\, J_{sf}\chi_{0s}/g^2\mu_B^2 N$; χ_{0s} taken as 55.8×10^{-6} emu/mole; $H_{\text{hfs}} = 0.45\times10^6$ Oe.

[d] $H_{\text{eff}}^{\text{hyb}} = [g_J/(g_J - 1)]\, N\mu_B\alpha_{\text{hyb}}$.

[e] $H_{\text{eff}}^{\text{hyb}} = 6H_{\text{hfs}}fs/(2S)$; $H_{\text{hfs}} = 0.45\times10^6$ Oe, $2S = 2$ for U^{4+}, $2S = 4$ for Pu^{4+}; f_s = fraction of unpaired spin (per actinide nearest neighbor).

sult of strong hybridization of the $5f$ wave function with the s-wave conduction electrons at the Fermi energy.[16] The contact hyperfine interaction is assumed to be responsible for the nuclear coupling. In our analysis we will assume that α_{ex} dominates in UAl_2 and α_{hyb} dominates in $PuAl_2$. That is, we believe that the fourfold increase in α at $PuAl_2$ relative to the value at UAl_2 is indicative of a much tighter coupling of the Al nucleus to the $5f$ electrons in $PuAl_2$. By comparison the isostructural rare-earth dialuminides[23] have values of α of order 1 mole/emu, which is typical of an effective exchange interaction.

Using a localized spin-fluctuation model,[11] the susceptibility in $PuAl_2$ is given by

$$\chi(q,\omega) = 2\mu_B^2(\hbar\omega_s + i\omega E_F/qv_F)^{-1} \quad , \tag{10}$$

where ω_s is the spin fluctuation frequency, E_F is the Fermi energy, and v_F is the Fermi velocity. It can be shown[9] that the spin-lattice relaxation rate is given in terms of the static susceptibility χ_0 by

$$(T_1T)^{-1} = (\alpha_{hyb}^2/2\pi S)\chi_0^2 \quad , \tag{11}$$

where S is the Korringa constant, $S = (\gamma_e/\gamma_n)^2 (\hbar/4\pi k_B) = 3.9 \times 10^{-6}$ (sec. °K)$^{-1}$.

In order to fit the experimental relaxation behavior in $PuAl_2$ we require a value of $\alpha_{hyb} = 9.9$ (erg/G^2)$^{-1}$ in Eq. (11). For UAl_2 we do not find a χ^2 dependence of $(T_1T)^{-1}$. Using α_{UAl_2} in Eq. (11), yields values of $(T_1T)^{-1}$ much smaller than found experimentally. We therefore assume $\alpha_{ex} = \alpha - \alpha_{hyb} = 1.3$ (erg/G^2)$^{-1}$ in $PuAl_2$ and linearly extrapolate α_{ex} with composition to the measured value in UAl_2, $\alpha = 2.9$ (erg/G^2)$^{-1}$, assumed to be entirely due to exchange (see Fig. 15).

In order to treat the effect of interband exchange coupling on T_1 in UAl_2, we use a molecular-field model to remove the effective exchange interaction between the f-band and s-band electrons. The results is an effective s-s interaction which yields an enhanced s-band susceptibility of the form

$$\chi_s(q,\omega) = \frac{\chi_s^0(q,\omega)}{1-(J_{sf}/g^2\mu_B^2N)^2\chi_s^0(q,\omega)\chi_f(q,\omega)} \tag{12}$$

where $J_{sf}/g^2\mu_B^2N = N\mu_B\alpha_{ex}/H_{hfs}\chi_s^0$.

The nuclear spin-lattice relaxation rate $1/T_1$ is proportional to $\omega_0^{-1}\Sigma_q\chi_s''(q,\omega_0)$, where ω_0 is the nuclear Larmor frequency. Equation (12) leads to a relaxation rate given by[9]

$$1/T_1 = 1/T_1^0\langle[1-(J_{sf}/g^2\mu_B^2N)^2\chi_s'^0(q,0)\chi_f'(q,0)]^{-2}\rangle \quad , \tag{13}$$

where the factor between the angular brackets is averaged over q vectors spanning the Fermi surface, and $1/T_1^0$ is the value of the relaxation rate for a noninteracting s band.

Equation (13) is evaluated[9] by averaging over a spherical Fermi surface using $\alpha_{ex} = 2.9$ (erg/G^2)$^{-1}$ for UAl_2. Approximating the q dependence of $\chi_f'^0(q,0)$ and $\chi_f'(q,0)$ by the Lindhard function gives a fair accounting of the dependence of $(T_1T)^{-1}$ on $\chi_f'(0,0)$ for UAl_2. For $PuAl_2$, Eq. (13) yields a negligible contribution to $(T_1T)^{-1}$ using $\alpha_{ex} = 1.3$ (erg/G^2)$^{-1}$.

In Table V we compare the values of the effective hyperfine fields per unit of spin H_{eff} at ^{27}Al in various dialuminides. Here H_{eff} is given by

$$H_{eff} = Ng_J\mu_B\alpha/(g_J-1) \quad . \tag{14}$$

We have taken the Russell-Saunders g values for the rare earths and assume a spin-only g value of 2 for the actinides. Because of the high degree of localization of the $5f$ state, the g value may, in fact, have quite a different value than 2. We note that the values of H_{eff} are negative for the rare-

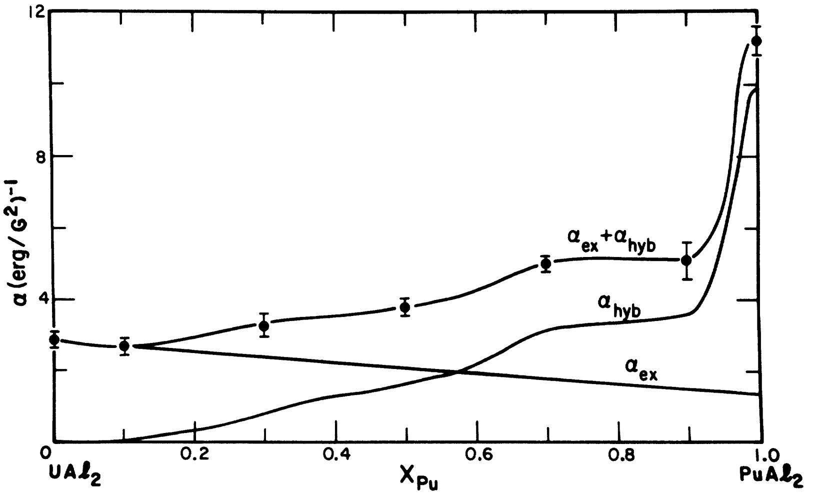

FIG. 15. Composition dependence of exchange and hybridization contributions to $\alpha \equiv dK/d\chi$ in $U_{1-x}Pu_xAl_2$.

earth dialuminides and positive for the actinide dialuminides. This indicates that the spin polarization at the aluminum site is antiparallel to the spin of the paramagnetic ion in the actinides.

Within the uniform spin polarization model, $H^{\mathrm{ex}}_{\mathrm{eff}}$ is related to the effective exchange coupling by

$$H^{\mathrm{ex}}_{\mathrm{eff}} = 2H_{\mathrm{hfs}}(J_{sf}/g^2\mu_B^2 N)\chi_{0s} \qquad (15)$$

where J_{sf} is the effective exchange interaction constant,[22] H_{hfs} is the contact hyperfine interaction in aluminum (0.45×10^6 G), and χ_{0s} is the uniform s-band susceptibility $\chi(0,0)$. Approximating χ_{0s} by three times the value in aluminum metal (55.8×10^{-6} emu/mole) consistent with the fit to $(T_1T)^{-1}$ in UAl$_2$, we find the values of J_{sf} shown in Table V.

Assuming the electron-nuclear interaction is of the contact type, the fraction of spin transfer f_s to the ^{27}Al site per actinide ion nearest neighbor is given by

$$H^{\mathrm{hyb}}_{\mathrm{eff}}/H_{\mathrm{hfs}} = 6f_s/(2S) \ , \qquad (16)$$

where H_{hfs} is taken as 0.45×10^6 G. There are six nearest-neighbor actinides to the Al, and $2S$ is the number of 5f electrons. The average number of 5f electrons associated with the virtually localized state is taken as 2 for U and 4 for Pu. The values of f_s (see Table V) appear to increase sharply near PuAl$_2$ to a maximum of about 0.16. The composition variation of $H^{\mathrm{hyb}}_{\mathrm{eff}}$ or f_s is consistent with the resistivity results. That is, hybridization of the s electrons with the f electrons at the Fermi energy increases dramatically with increasing Pu concentration. The lack of hybridization for $x \leq 0.1$ may be due to insufficient overlap of 5f wave functions associated with the plutonium ions. That is, the lack of formation of this band at dilute Pu concentration prevents the establishment of hybridization with the s band.

3. Inhomogeneous Magnetic Broadening of PuAl$_2$

The Curie-Weiss-type plot of excess linewidth in Fig. 14 yields

$$\Delta H - 50 = \frac{526 \text{ Oe} - {}^\circ\text{K}}{T - 4\,{}^\circ\text{K}} = \frac{CH}{T-\Theta} \qquad (17)$$

at an applied field of 10.8 kOe, where C is the Curie constant. If we assume for a computational estimate that the defect associated magnetic moment couples to the Al nucleus in PuAl$_2$ with the same transferred hyperfine coupling that characterizes the Knight-shift susceptibility relation, then we can divide the Curie constant by the value of α for PuAl$_2$ (see Table III). We find $cp^2_{\mathrm{eff}} \equiv (C/\alpha) \times (N\mu_B^2/3k_B)^{-1} = 0.034$. That is, the observed linewidth in PuAl$_2$ at low temperatures could result from a distribution of "impurity" moments. If the "impurity" had an effective moment $p_{\mathrm{eff}} = 1$ (in units of the Bohr magneton), the concentration c would be of order 3 at.%. In fact, the impurity in the present case may be a region of crystallographic disorder rather than another chemical element. The above treatment is intended to give only an order of magnitude estimate for the impurity moments.

V. CONCLUSIONS

The results of resistivity, susceptibility, Knight shift, and nuclear spin-lattice relaxation in Pu-rich U$_{1-x}$Pu$_x$Al$_2$ compounds are consistent with a picture of an s band strongly coupled to a virtually localized state (assumed to be of 5f character) at the Fermi level. For the uranium-rich compounds the 5f state is centered well off the Fermi level and the coupling to the s-wave conduction electrons at E_F is small. In PuAl$_2$ the coherence of the s-f hybridization is destroyed by spin-fluctuation scattering above 10 °K. Atomic disorder, due to radiation damage or chemical substitution, destroys the coherence at all temperatures. The loss of coherence causes resonant virtual-bound-state formation in the Pu-rich compounds. Eventually, as temperature is increased spin-fluctuation scattering causes the virtual-bound states to shift off resonance yielding negative values of $d\rho/dT$.

The relatively constant value of qa_0^3 in the U$_{1-x}$Pu$_x$Al$_2$ compounds indicates a similar valence state (point charge) for uranium and plutonium. Thus a plutonium ion has approximately two more 5f electrons localized in real space than does a uranium ion. As the plutonium concentration increases the effective moment decreases. This may be due, in part, to broadening of the 5f state resulting from increased overlap between the 5f wave functions of the Pu ions as x increases. Broadening and overlap of the spin split 5f states is consistent with the drop in χ_{orb} for $x \geq 0.9$. However, the s-f hybridization at the Fermi level increases with increasing plutonium concentration. The result is a peak in magnetic-ordering temperature at intermediate concentration, i.e., near $x = 0.3$. Local regions of short-range magnetic order may also occur for large x associated with crystallographic disorder.

Finally, we note that the 5f electrons of the actinides experience both strong spin-orbit coupling (as do the 4f electrons of the rare earths) and strong crystalline electric field interactions (as do the outer d electrons of the transition metals). The competition between atomic and bandlike behavior of the 5f electrons is highly sensitive to its crystallographic environment. This leads to well localized bound states in the actinide NaCl-type compounds and relatively weak spin-fluctuation behavior of itinerant 5f electrons in the actinide metals. The actinide-cubic Laves phases have intermediate magnetic behavior, characterized by virtual-bound state formation and strong spin-fluctuation phenomena.

ACKNOWLEDGMENTS

We wish to thank Dr. S. Doniach for showing us his manuscript prior to publication and for many stimulating discussions. Numerous discussions with Dr. W. J. Nellis, Dr. A. R. Harvey, Dr. G. H. Lander, Dr. M. H. Mueller, and Dr. D. J. Lam are greatly appreciated. Special thanks go to Dr. D. J. Lam for critically reading this manuscript. We also wish to thank C. H. Sowers and N. Griffin for technical assistance.

[†] Work performed under the auspices of the U. S. Atomic Energy Commission.

[1] R. Jullien, E. Galleani d'Agliano, and B. Coqblin, Phys. Rev. B **6**, 2139 (1972).

[2] B. D. Dunlap, M. B. Brodsky, G. M.Kalvius, G. K. Shenoy, and D. J. Lam, J. Appl. Phys. **40**, 1495 (1969).

[3] A. C. Gossard, V. Jaccarino, and J. H. Wernick, Phys. Rev. **128**, 1038 (1962).

[4] A. J. Arko, M. B. Brodsky, and W. J. Nellis, Bull. Am. Phys. Soc. **15**, 293 (1970).

[5] F. Y. Fradin, M. B. Brodsky, and A. J. Arko, J. Phys. (Paris) **32**, 60 (1971).

[6] A. J. Arko, M. B. Brodsky, and W. J. Nellis, Phys. Rev. B **5**, 4564 (1972).

[7] M. B. Brodsky, Phys. Rev. **137**, A1423 (1965); in *Plutonium 1965*, edited by A. E. Kay and M. B. Waldron (Chapman-Hall, London, 1967), p. 286.

[8] F. Y. Fradin and D. Zamir, Phys. Rev. B **7**, 4861 (1973).

[9] F. Y. Fradin, A. J. Arko, and M. B. Brodsky, AIP Conf. Proc. 10, 192 (1973).

[10] A. B. Kaiser and S. Doniach, Int. J. Magn. **1**, 11 (1970).

[11] S. Doniach, AIP Conf. Proc. 5, 549 (1972).

[12] S. Doniach, in *Electronic Structure and Related Properties of the Actinides*, edited by A. J. Freeman and J. B. Darby (Academic, New York, to be published).

[13] M. H. Cohen and F. Reif, in *Solid State Physics*, edited by F. Seitz and D. Turnbull (Academic, New York, 1957).

[14] S. J. Langer and S. H. Vosko, J. Phys. Chem. Solids **12**, 196 (1959).

[15] R. E. Watson, A. C. Gossard, and Y. Yafet, Phys. Rev. **140**, A375 (1965).

[16] R. E. Watson and A. J. Freeman, in *Hyperfine Interactions*, edited by A. J. Freeman and R. B. Frankel (Academic, New York, 1967), p. 53.

[17] R. G. Barnes and R. G. Lecander, J. Phys. Soc. Jap. **22**, 930 (1967).

[18] R. M. Sternheimer, Phys. Rev. **146**, 140 (1966).

[19] F. Herman and S. Skillman, *Atomic Structure Calculations* (Prentice-Hall, Englewood Cliffs, N. J., 1963).

[20] V. Jaccarino, B. T. Matthias, M. Peter, H. Suhl, and J. R. Wernick, Phys. Rev. Lett. **5**, 251 (1960).

[21] W. H. Jones, Jr., T. P. Graham, and R. G. Barnes, Phys. Rev. **132**, 1898 (1964).

[22] R. E. Watson, in Ref. 16, p. 413.

[23] E. D. Jones, Phys. Rev. **180**, 455 (1969).